Research in Astron. Astrophys. **2013** Vol. **13** No. **10**, 1240–1254
http://www.raa-journal.org *http://www.iop.org/journals/raa*

Research in Astronomy and Astrophysics

The first observation and data reduction of the Multi-wavelength Spectrometer on the New Vacuum Solar Telescope *

Rui Wang[1,2], Zhi Xu[1], Zhen-Yu Jin[1], Zhi Li[1], Yu Fu[1] and Zhong Liu[1]

[1] Yunnan Astronomical Observatory / National Astronomical Observatories, Chinese Academy of Sciences, Kunming 650011, China; *xuzhi@ynao.ac.cn*
[2] University of Chinese Academy of Sciences, Beijing 100049, China

Received 2013 March 5; accepted 2013 May 20

Abstract The Multi-wavelength Spectrometer is a medium-dispersion ($R \sim 130\,000$) grating spectrometer installed on the New Vacuum Solar Telescope at the Fuxian Solar Observatory, Yunnan Astronomical Observatory, Chinese Academy of Sciences. It is designed to accurately observe the velocity and magnetic fields of the Sun. The present configuration of this spectrometer allows us to simultaneously observe three different solar spectral lines. This work is dedicated to showing the first observations carried out in both the Hα and Ca II 8542 Å lines. We give a detailed description of the data reduction process, focusing on the retrieval of a flat field from the high-resolution spectral data. Two different methods are also performed and compared to eliminate the residual fringe in the reduced data. The real spectral resolution and instrumental profile are analyzed based on the final results, which indicate that this spectrometer presently satisfies the expected performance and it is ready for further scientific observations.

Key words: instrumentation: spectrographs — techniques: spectroscopic — Sun: chromosphere

1 INTRODUCTION

The New Vacuum Solar Telescope (NVST) at the Yunnan Astronomical Observatory has an Alt-Az mounting and an aperture of 980 millimeters. The effective focal length is about 45 m and the field-of-view is about $3'$. The main goal of the NVST is to observe the Sun in the range of 0.3–2.5 μm (Liu & Xu 2011) using high resolution imaging systems and spectrometers with a polarization analyzer. There are two vertical spectrometers working in different visible and infrared lines. They are the Near Infrared High-dispersion Spectrometer and Multi-wavelength Spectrometer. Here we give a detailed description of the present status of the Multi-wavelength Spectrometer before the polarization analyzer is installed.

The Multi-wavelength Spectrometer is a medium-resolution spectrometer with a theoretical spectral resolution ($\lambda/\Delta\lambda$) of 1.3×10^5. The basic optical layout is illustrated in Figure 1. The installation was completed in 2011 (Fu et al. 2012). The main properties of this spectrometer are listed in Table 1. Three CCD cameras (2672×4008 pixels) are installed in the focal plane, allowing simultaneous observations in three different wavelengths. The present channels are configured to be

* Supported by the National Natural Science Foundation of China.

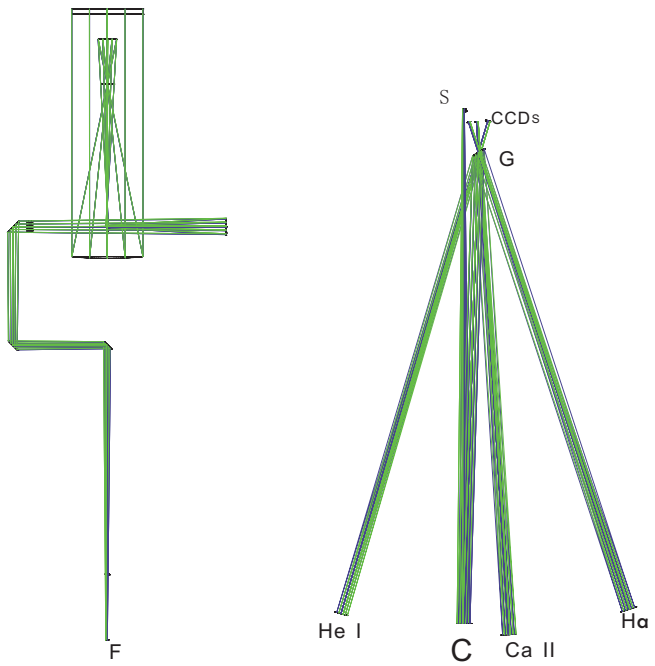

Fig. 1 *Left*: Full optical path of the New Vacuum Solar Telescope from the vacuum window to the telescope focal plane (F), where the Multi-wavelength Spectrometer is installed. *Right*: optical layout of the vertical and Multi-wavelength Spectrometer, including the slit (S), collimator mirror (C), grating (G), three imaging mirrors in three channels (denoted by He I, Hα and Ca II, respectively) and the cameras (CCDs).

Table 1 Main Properties of the Multi-Wavelength Spectrometer

Spectrometer	blazed grating (rotatable)
Grating size	156 mm×220 mm
Grooves per mm	1200 g mm^{-1}
Blazed angle [°]	36.8 (1st order, blazed wavelength 10000 Å)
Present slit width [μm]	90 (0.45 ″)
Linear dispersion [mm Å^{-1}]	0.75 @ Hα, 0.82 @Ca II 8542, 1.09 @ He I 10830
	2 @ Fe I 5250 & Fe I 5324
Frame size of raw spectra [pixel]	2672×4008
Pixel size [μm]	9×9
Spectral sample [mÅ pixel^{-1}]	12 @ Hα 6563, 11 @ Ca II 8542, 8 @ He I 10830
	4.5 @ Fe I 5250 & Fe I 5324
Spatial sample [arcsec pixel^{-1}]	0.041

centered at the Hα, Ca II 8542 Å and He I 10830 Å lines (which can be converted to the Fe I 5250 Å line pair or Fe I 5324 Å line) with a coverage of 40–50 Å. A set of data reduction routines especially suited for spectral data taken with the NVST has been developed. In this paper, we introduce the data reduction process step by step, emphasizing the retrieval of a 2D flat field. Additionally, some special problems beyond the regular reduction, e.g., the elimination of residual fringes in the reduced data, are also discussed in detail.

Generally speaking, the goal of data reduction is to remove the artifacts imposed by the observing system from the 2-dimensional spectral image (Scodeggio et al. 2005). The observing system here refers to the telescope, detectors and optical elements of the spectrometer. The standard process can be simply described by the following equation

$$R = \frac{S - K}{F - K}\,, \tag{1}$$

where R represents the reduced spectral data. S represents the raw object data. K and F are the background frame and flat field, respectively. The background frame K comprises three components of noise which add analog-to-digital units (ADUs) to the read out noise of every frame. The sources of this noise are the bias level, dark current and scattered light. A detector always produces positive values when it is read out even with zero-time exposure and zero light input. The positive output that occurs with an exposure of no duration is called the bias level. The dark current is primarily a thermal effect and proportional to $T^{3/2}\mathrm{e}^{(-a/kT)}$, where a is a constant and T is the temperature (Howell 2006). A scientific CCD is usually cooled with liquid nitrogen to minimize thermal effects. As a result, the dark response can be negligible even with a long exposure time. Scattered light comes from light surrounding the instrument. In solar observations, one actually obtains a background composed of all these three components in one exposure.

The flat field is used to calibrate the non-uniform response of the CCD camera since not all pixels have an equal response efficiency with respect to incoming radiation. This can result from differences in the gain and quantum efficiency of different pixels throughout the surface of the chip. It can also arise from optical vignetting, dust laying on the camera window, the finite travel time of the shutter across the field of view, etc. For a spectrometer, there exist some additional sources including imperfections in the entrance slit and dust on it (see Wöhl et al. 2002). Sometimes the fringe is another serious problem that needs to be taken into account, especially for observations in infrared wavelengths.

There are many methods to obtain the so-called flat-field source frame from which one can extract the flat field. Generally, there needs to be a light source that uniformly illuminates the whole two-dimensional view of the camera (e.g., the skylight at dawn or light reflected by the telescope dome is widely used in night observations). In addition, the light source should have an identical spectral emission distribution as that of the object. A quartz or other high-intensity projector lamp is sometimes used as a light source in the spectroscopic observation to illuminate the entrance slit, and then the grating (Howell 2006). In this case, the spectral range of the flat-field source frame needs to precisely match that of data from the object since the response of the camera depends on wavelength. In observations related to solar spectroscopy, a light source used for flat-field observation should be as strong as sunlight with the same continuous spectrum. It is impossible to get such an ideal light source, so the Sun itself is used instead. Two popular methods are often used to obtain the flat-field source frame. (1) Defocus the telescope or open the slit to a quite large width in order to make the image sufficiently un-sharp. Then a few frames are obtained and averaged to create a flat field. However, the disadvantages due to defocusing are clear. It obviously changes the optical setup, and consequently, artifacts such as fringes will change their patterns. Most importantly, it tends to smear out the non-uniform response caused by defects in the silt, dust on the slit, and other problems due to the defocusing method itself (e.g., Johanneson et al. 1992; Hall et al. 1994). (2) Acquire the flat-field source frame in the same way as data from the object with the same spectral resolution, followed by removing the features of spectral lines to obtain the final flat field (e.g., Kiselman 1994; Bommier & Molodij 2002). It is more convenient to use the second one since the observer does not need to adjust any optical setup during the whole observation. Through this process, the non-uniform response produced by the whole observing system is well recorded. Therefore we employ the second method to retrieve the final flat field in spectral observations with the NVST. We will describe the retrieval process in detail in the data reduction section (Sect. 2.2.3).

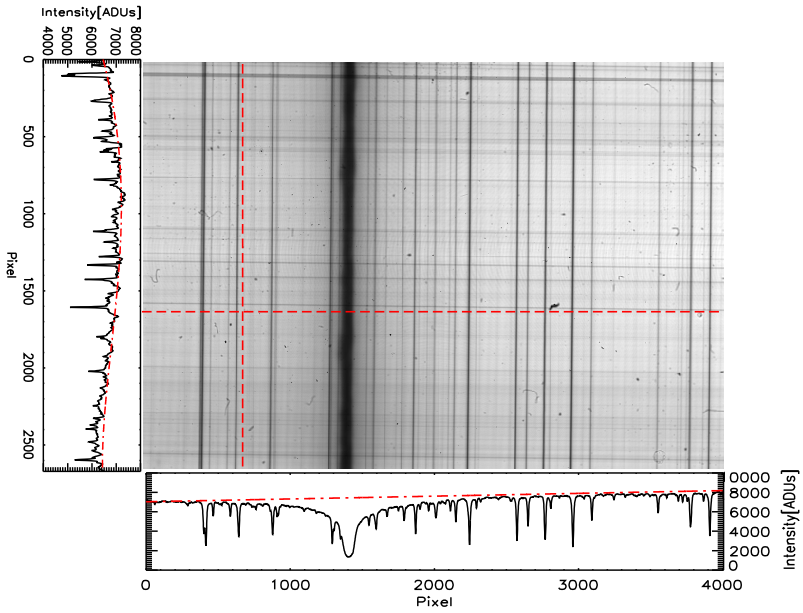

Fig. 2 Typical raw data of the Hα line observed at the solar disk center using the NVST on 2012 July 31. Two orthogonal dashed lines are parallel to the row and column axis, respectively, as a reference for the image curve. It is shown that this 2D spectral image has geometric distortion along these two directions. The left (*bottom*) panel shows the mean profile averaged along the row (*column*) axis. The dot-dashed lines over the mean profile indicate the general variations in intensity.

This paper is organized as follows. In Section 2, we illustrate the data reduction process step by step. In Section 3, we discuss the relationship between the number of flat-field source frames and the quality of the flat field. In addition, we discuss two methods to suppress the residual fringe in the reduced data. In the last section, we draw a conclusion about the main properties of the data reduction, which can be used as a good reference for the spectroscopic observations made with the NVST. The performance of the Multi-wavelength Spectrometer is also evaluated in this section.

2 DATA REDUCTION

A set of spectral data was obtained with the Multi-wavelength Spectrometer at a quiet area near the solar disk center on 2012 July 31. Both the Hα and Ca II 8542 Å lines were simultaneously observed. An entrance slit of 180″ long and 0.45″ (90 μm) wide was used to measure the typical spectral resolution (12 mÅ/pixel in the Hα channel), conjoined with the digital Hα slit-jaw image. A total of 500 frames of the object spectrum were observed with an exposure time of 200 ms in the Hα channel and 1 s in the Ca II channel.

Figure 2 shows an example of object data in the Hα channel, which exhibits five obvious problems in the raw data.

(1) Blemishes that are mainly caused by dust on the optical setup and camera window.
(2) Horizontal dark lines produced by dust on the slit, mixed with some solar absorption structures (e.g., sunspots or pores).
(3) The geometric curvature along both the slit and dispersion directions that have different slopes.

(4) A gentle variation in brightness along the spatial and dispersion directions seen in the left and bottom panels.
(5) Fringes in different patterns.

2.1 Background Correction

In general, the background may vary during the observation run. One reason is that both the bias level and dark response change with variations in temperature. The scattered light could also change when the setup of the instrument changes. Hence, one should obtain the background and object data in a similar environment in order to minimize the influence of variations in the background. We did the following experiment in our observation on July 31.

We firstly obtained two groups of background data in the morning before the daily observation. Each group contains 20 frames. One group was obtained by shutting the CCD camera (e.g., with exposure time of zero). The other was made with a 20 ms exposure by covering the entrance slit (e.g. with zero light input). For each group, we performed unsharp masking on each frame in order to eliminate the cosmic-ray hits and other uncertainties. The 20 frames were averaged to construct one master background for both groups, (K). It was found that the mean values of these two master backgrounds were almost the same, regardless of whether we shuttered the camera or covered the slit. We repeated this observation and the data reduction above in the afternoon after the daily observation and found a similar result, which indicates that the background does not significantly change with time. For convenience we prefer to acquire the background by covering the entrance slit when we finish the daily observation. For the dark correction, the master background (K) is subtracted from the given sequence of object data frames and flat-field source frames.

2.2 Flat-field Correction

2.2.1 Acquisition of source frames and construction of the mean flat-field source frame

The flat-field source frames were observed by pointing the telescope to a quiet region near the solar disk center and moving it randomly within approximately $3' \times 3'$. The purpose of this is to avoid the same solar position passing through the slit several times. 500 frames of the flat-field source data were obtained in the Hα and Ca II 8542 Å channels, with the same exposure time as the object data. We carried out the flat-field observation as soon as we completed observation of the object.

In spite of the special movement mode of the telescope, the flat-field source frame still contains some solar structures. For instance, we can clearly recognize some emission or absorption features due to Ellerman bombs or small pores. Some relatively large Doppler velocities are also seen in some frames. Therefore, it is necessary to acquire one *mean flat-field source frame* by using the multi-frame average. Firstly, we calculate the so called intensity proxy of each frame. The intensity proxy is constructed by averaging five pixel values (it is noted that the positions of these five pixels are exactly the same in each frame). The temporal sequence of the intensity proxy is given in Figure 3. These frames, whose intensity proxies deviate from their mean value by more than 15%, are rejected or neglected. Among the 500 frames in our observation, seven bad frames are detected using this criterion, which may be due to cloud cover at that time. However, we only select and average 200 successive frames instead of 493 $(= 500 - 7)$ frames to construct the *mean flat-field source frame*. In the Discussion section, we will consider the effect of the number of source frames on the quality of the final flat field.

2.2.2 Rectifications of the mean flat-field source frame

The *mean flat-field source frame* presents a different curvature along the slit and dispersion directions (as shown in Fig. 2). This is a common problem for spectral observations. It can be interpreted as

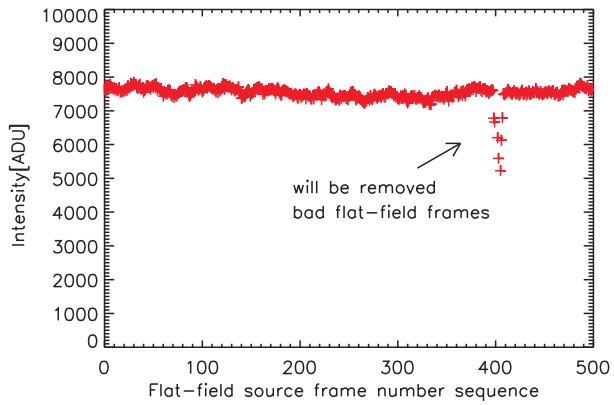

Fig. 3 Temporal sequence of the intensity proxy of the flat-field source frame. "Bad" frames (see the definition in the text) are indicated by an arrow.

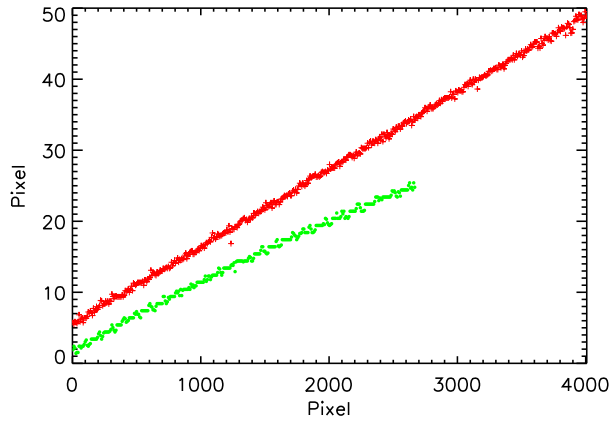

Fig. 4 The spectral image curvatures along both the slit and dispersion directions. The x axis represents the pixel number. The y axis means the relative displacement of position for line centers. The positions of line centers for a certain spectral line along the slit direction are shown with green filled circles. The relative displacement of the line centers of one horizontal dark line along the direction of dispersion is shown with red pluses.

the geometric bend in the entrance slit itself or the position of the slit relative to the direction of the grating grooves, as well as other possible reasons. The first and most important step is to accurately rectify the *mean flat-field source frame* in two dimensions. In this section, we show our method to measure and de-stretch the spectrum in the slit and dispersion directions.

We determine the image curvature along the slit direction (vertical axis) by taking advantage of several solar spectral lines within the *mean flat-field source frame*. One spectral line on the left side of the frame is selected. In each row, the position of the line center is determined by using a third-order polynomial fit to 20 points around the central part of the line profile. The pixel displacements of the position of the line center along the slit are presented in Figure 4 (green filled circles). By trial and

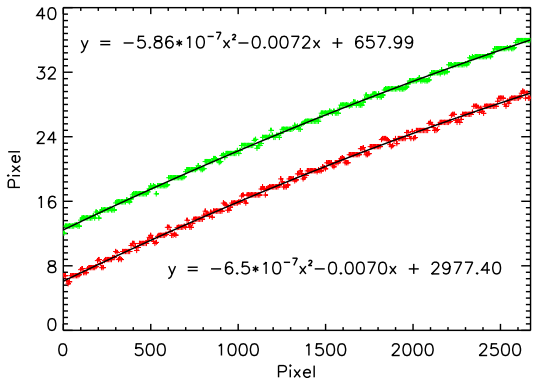

Fig. 5 Pixel displacements of the line center positions along the slit direction for two spectral lines. Their best-fit polynomial curves are also given.

error, it is found that a second-order polynomial can best fit this distribution. The standard deviation between the observation and fit is 0.36, which is smaller than the value of 0.52 derived from a linear fit. Then another spectral line on the right side of the frame is utilized to repeat the detection of the line center position. The pixel distance between these two lines covers more than 2/3 of the CCD's horizontal axis. Both the positions of their line centers and the best-fit polynomial are displayed in Figure 5. Despite the small deviation between their polynomial coefficients, these two lines are almost parallel to each other, which means that the curvature along the slit direction is independent of line position. As a result, a narrow, strong absorption line, whose line center position is more easily and reliably detected by our method, is selected to measure the curvature along the direction of the slit. Similarly, we choose a horizontal dark line located at the top of the frame to determine the curvature along the dispersion direction (horizontal axis). This measurement can be done using the dark line due to the *spider line* on the entrance slit. Here we use one horizontal dark line caused by dust on the slit. In each column, a third-order polynomial fit is also applied to find the position of the dust line. The pixel displacement of the position for the dust line along the dispersion direction is plotted in Figure 4 (red pluses), and a linear function is enough to fit this curve. The curvature of the image along the dispersion is also found to be independent of line position (not shown in the plot). From Figure 4, it is clearly seen that the *mean flat-field source frame* has different curvatures in two dimensions. It slightly bends along the slit orientation but inclines along the dispersion direction.

Based on the measurement above, we divide our 2D de-stretching into two steps. Firstly, one horizontal dark line is selected and its trend in inclination is fitted with a linear function. A tilt angle between this linear function and the horizontal axis is calculated. The *mean flat-field source frame* is rotated by using bilinear interpolation according to this tilt angle. Secondly, a narrow, strong absorption line is utilized to detect the curvature along the slit direction. Then this curvature is rectified by shifting the line position, column by column, according to this best-fit polynomial (not the scattering data set itself). As a result, the direction for dispersion is strictly parallel to the horizontal axis and perpendicular to the slit direction. One example of the *mean flat-field source frame* after 2D de-stretching is shown in the left panel of Figure 6.

2.2.3 Flat field retrieval

The purpose of this step is to remove the spectral line from the rectified *mean flat-field source frame* by using the *mean profile* method (Bommier & Molodij 2002; Bommier & Rayrole 2002). The *mean*

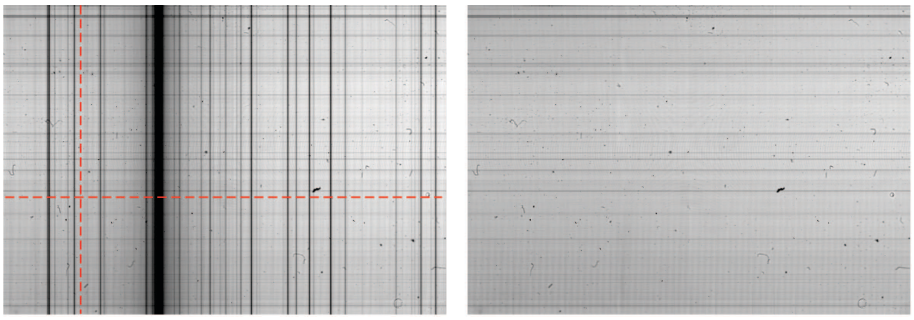

Fig. 6 *Left*: The *mean flat-field source frame* after 2D geometric rectification. A horizontal (vertical) dashed line indicates the dispersion (slit) direction. *Right*: an example of the 2D flat field in the Hα channel. Some weak non-uniform responses due to the remnants of spectral line features still exist.

profile is obtained by averaging the rectified *mean flat-field source frame* along the slit direction. Researchers have found that sometimes it is better to average over part of the slit rather than the whole slit in order to avoid the influence of some large blemishes with pixel values close to zero. As seen in Figure 2, there is a light variation in the intensity for the continuum of the *mean profile*. We select a few points in the continuum over the entire dispersion direction. A linear fit is used to find the trend in variation for the continuum intensity. Then the *mean profile* is linearly modified according to the best-fit linear function. Finally, the rectified *mean flat-field source frame* is divided by the continuum corrected *mean profile*. Features of all spectral lines are completely eliminated. The flat field is ultimately retrieved as shown in the right panel of Figure 6.

2.2.4 Flat-fielding the object data

First of all, the object data after background subtraction should be rectified in exactly the same way as for the *mean flat-field source frame*. Secondly, the object data are divided by the flat field according to Equation (1). An example of flat-fielded data is illustrated in Figure 7, which is actually the result of reducing the data shown in Figure 2. Most of the non-uniform responses on the object data, as described in Section 2, are removed by the flat-field correction. Some fringes behaving like solar spectral lines still remain, particularly in the case of observations at long wavelengths. Methods to eliminate the remaining fringes are proposed in the Discussion section.

2.2.5 Wavelength calibration and evaluation of the instrumental profile

To do the wavelength calibration of the reduced data, a spectrum from the FTS atlas is utilized (FTS is a spectrum from the atlas obtained by a Fourier Transform Spectrometer at the McMath/Pierce Solar Telescope). Normally, telluric lines are recognized and used to determine the wavelength calibration by assuming that the central position of the telluric line corresponds to the laboratory wavelength. The real dispersion resolution (or spectral sample) of our spectrometer is also inferred in this way. The spectral sample is derived to be about 0.011 Å/pixel, very close to the expectation (listed in Table 1). We present a reduced and wavelength calibrated Hα line (red) superposed on the FTS atlas spectrum (black) in Figure 8. It can be seen that the observed solar spectral lines are slightly shallower than the FTS spectrum, due to the contamination of stray light from the spectrometer. However, the observed telluric lines have stronger absorption than those given by the FTS atlas.

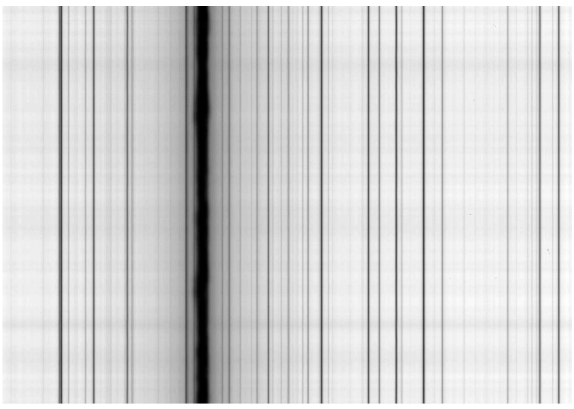

Fig. 7 An example of reduced data in the Hα channel. It is actually the result of reducing the spectral data of the object shown in Fig. 2.

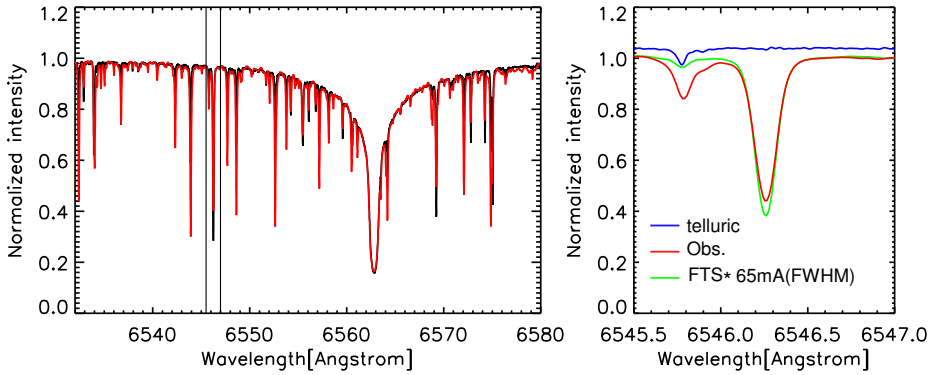

Fig. 8 *Left*: A comparison between the reduced spectral profile in the Hα channel (*red line*) and the FTS atlas spectrum (*black line*). *Right*: Enlargement of part of a solar spectrum, whose range is delimited by two vertical lines in the left panel. The telluric line is shown in blue to reveal that the line in the center of this panel is a solar spectral line. The observed line and the FTS convolved with a Gaussian profile are shown in red and green, respectively.

In fact, the observed spectrum is the combination of the real spectrum and the instrumental profile. Assuming that the instrumental profile is a Gaussian profile, we find that the FTS spectrum needs to be convolved with a Gaussian profile, whose full width at half maximum (FWHM) is about 0.065 Å, in order to precisely match our observation. In the right panel of Figure 8, we demonstrate this influence by using a very narrow solar spectral line, whose observed FWHM is less than 0.2 Å. We roughly infer that the upper limit of the FWHM for our instrumental profile is 0.065 Å considering that there exist some other spectral broadening mechanisms.

In brief, the standard routines in Section 2 are generally sufficient for reducing data from the object. However there still exist some residual artifacts in the reduced data, for example, the special fringe we mentioned above. Some additional treatments are needed, particularly for the Ca II 8542 Å line. We will discuss how to avoid and eliminate these residual artifacts in the following section.

3 DISCUSSION

Flat-field correction plays a more important role than other processes. In this section we focus on two aspects related to the flat-field correction. One is the residual spectral feature on the flat field. The other is the residual fringe in the reduced data after flat-fielding.

3.1 Influence of the Number of Flat-field Source Frames on the Flat field Retrieval

It is crucial to acquire a sufficient number of flat-field source frames in order to weaken the particular solar dynamic structure, including small pores, Ellerman bombs or other structures with large Doppler velocities. As we mentioned in Section 2.2.1, 493 good frames are obtained in total (seven bad frames are rejected). But only 200 continuous frames are used for the flat field retrieval.

Figure 9(a), 9(b) and 9(c) shows three different flat fields retrieved from 10, 220 and 493 source frames, respectively. Using 10 source frames, the residual spectral feature (e.g. the Hα line) is still clearly seen in the flat field. It becomes weak if we increase the number of source frames. However there is no obvious improvement as we increase the number of frames from 220 to 493. In Figure 9(d) we plot the residual spectral profile averaged over the partial slit, indicated by the box shown in Figure 9(a). We calculate the standard deviation between the residual spectral feature and the surroundings that do not have spectral features, σ_N (where N represents the number of source frames). The results are σ_{10} = 0.0523, σ_{120} = 0.0266, σ_{220} = 0.0221, σ_{340} = 0.0219 and σ_{493} = 0.0220. It is seen that the standard deviation is significantly reduced to 0.0266 when the number of source frames is increased to 120, but after that the improvement is not obvious. For the purpose of saving time, we employ about 200 frames covering three minutes to retrieve the flat field.

3.2 Elimination of the Residual Fringe

For our spectrometer, the main reason for fringes is similar to the case of thin-film interference due to the thickness of the camera window (Malumuth et al. 2002). Fringes superposed on the object data can generally be eliminated to a large degree after flat-fielding, as long as the flat-field source frame and the object data are taken at close intervals.

In Figure 10, different parts of data before and after flat-fielding are zoomed in to illustrate the effect of eliminating different patterns of fringes. However, it is noted that a fringe pattern behaving like solar spectral lines (i.e. the vertical fringe) cannot be eliminated after flat-fielding. In the case of the Ca II 8542 Å line, the residual fringe even gives rise to a fluctuation in intensity of the continuum, up to 12%. Therefore, an extra step for correction is needed after the standard reduction to remove the vertical fringe in the reduced data.

We apply two different methods according to the different appearance of the vertical fringe in the Hα and Ca II 8542 Å channels. Both methods have to use the *mean profile* derived from the rectified *mean flat-field source frame*. This is because the vertical fringe cannot be eliminated by the flat field retrieved using the *mean profile* method, so we need to extract the vertical fringe from the *mean profile*.

The first method described by Pereira et al. (2009) and Allende Prieto C. et al. (2004) is favorable for the Ca II 8542 Å line. As shown in the left panel of Figure 11, many spectral lines around the Ca II 8542 Å line have a narrower line width than the vertical fringe. In this case, we firstly obtain the ratio between the spectrum in the FTS atlas and the *mean profile*. The ratio is then smoothed and referred to as a correction spectrum (Pereira et al. 2009). The object data after flat-fielding need to be divided by this correction spectrum, and the residual fringe is eliminated. We present the de-fringed result in the right panel of Figure 11. For a careful comparison, the one-dimensional line profile of the flat-fielded spectrum (the dark line), the corrected spectrum (the green line) and the de-fringed spectrum (the red line) are plotted in Figure 12.

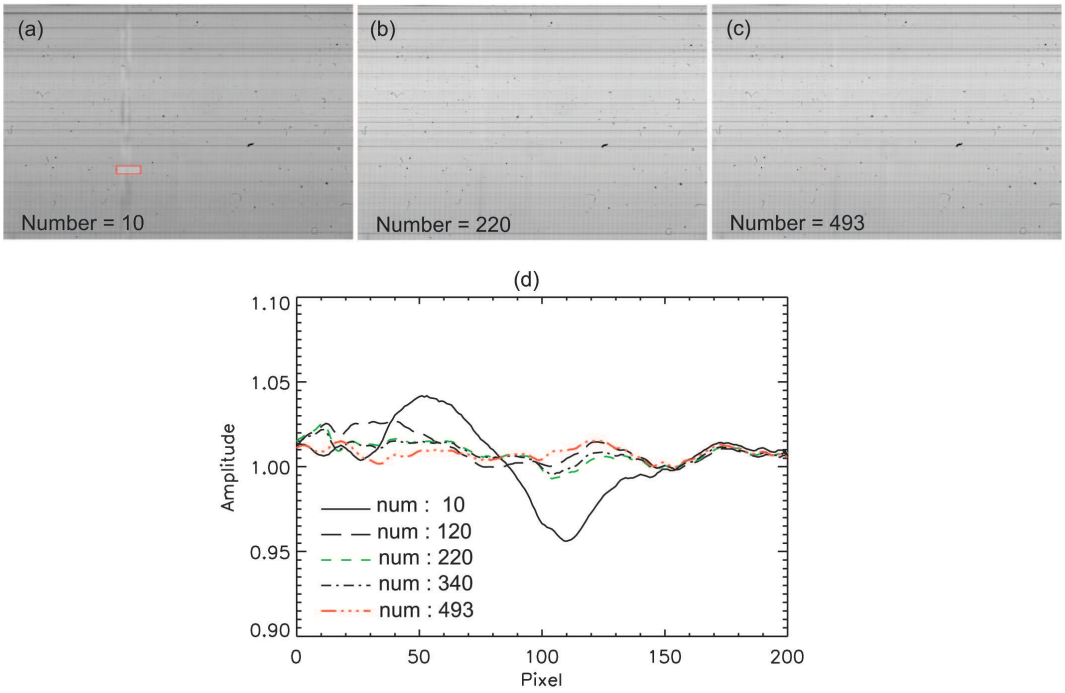

Fig. 9 Panels (a), (b) and (c): Flat fields of the Hα channel retrieved from 10, 220 and 493 source frames, respectively. Panel (d): The residual spectral feature averaged along the vertical direction of the area indicated by a box. The spectral features due to the different numbers of source frames are represented by different line styles.

However, the above method is useless in the case of the Hα channel because the width of the vertical fringe is comparable to the line widths of many spectral lines. Here we propose to use wavelet analysis to probe the vertical fringe. We use another set of Hα observations taken in January, 2012, that shows a stronger fringe than the one obtained on 2012 July 31. The residual fringe gives rise to the fluctuations in intensity for the continuum of up to 4.2%. We illustrate the reduced data in the left panel of Figure 14 over-plotted with the spectral profile. One can easily see the vertical fringe in the continuum. The following modification of the *mean profile* is needed to eliminate the absorption lines but keep the fringes: the points whose intensities are lower than 90% of the averaged continuum intensity are replaced by using an interpolation from the nearby points. Then, we apply the wavelet transform to the modified *mean profile* and the power spectrum is shown in the upper panel of Figure 13. It is seen that there is a prominent period around the 55th pixel along the X axis that has a certain spread. We regard the 55th pixel as a reference period. Following the algorithm developed by Rojo & Harrington (2006), we isolate this power spectrum by finding the first local minima on both sides of the reference period (their positions are indicated by two white curves). A Gaussian profile is used to fit the power spectrum inside the local minima. The period corresponding to the Gaussian peak is plotted with a thin dark line. The power spectrum outside the local minima is set to be zero. As a result, we obtain a modified power spectrum. Next, we apply an inverse wavelet transform to the modified power spectrum to reconstruct the fringe. The amplitude of the reconstructed fringe along the dispersion direction is plotted in the bottom panel of Figure 13. Eventually, the reconstructed fringe comes from the object data after flat-fielding and needs to be

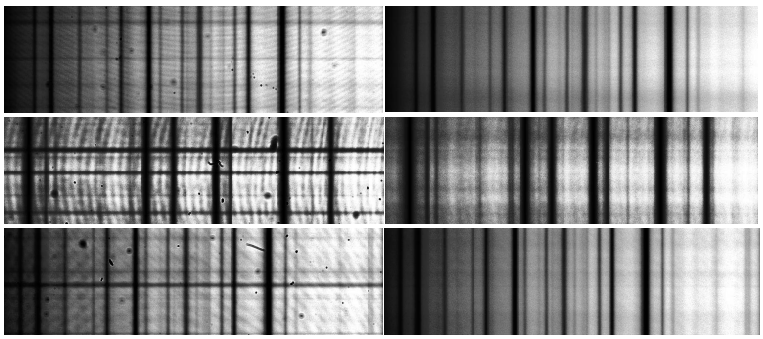

Fig. 10 Different sub-areas of the Hα spectral data before (*left*) and after (*right*) flat-fielding to exhibit the effect of eliminating the different fringes. From top to bottom, they are cases of the upward arc-shaped, leftward arc-shaped and downward arc-shaped fringes, respectively.

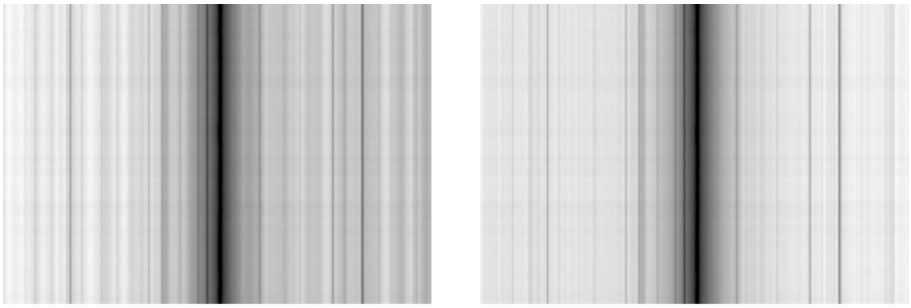

Fig. 11 A comparison of the reduced data in the Ca II 8542 Å line before and after the elimination of the residual fringe using the method to produce a corrected spectrum (see the definition in the text).

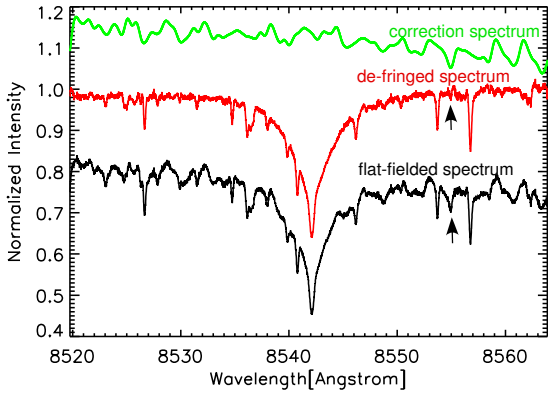

Fig. 12 A comparison of the flat-fielded spectrum (*black line*), correction spectrum (*green line*) and de-fringed spectrum (*red line*). In this plot, the de-fringed spectrum is normalized. The correction spectrum and flat-fielded spectrum are plotted in random units for comparison. The arrows indicate the disappearance of a telluric line after de-fringing.

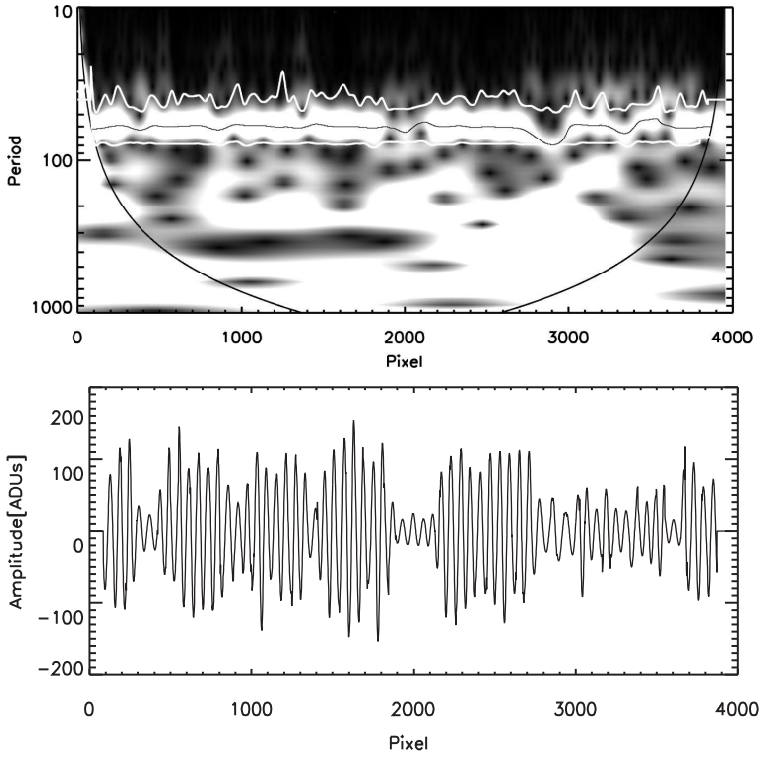

Fig. 13 *Top*: The power spectrum of the wavelet transform (WPS) of the modified *mean profile* shown in the left panel of Figure 14. The edge of the cone of influence is shown by a thick black curve. Two horizontal white lines demarcate the position of the first local minimum around the period of the 55th pixel. The power spectrum outside the two lines are set to be zero. The final period determined by a Gaussian fit is plotted as a thin black line. *Bottom*: The amplitude of the reconstructed fringe along the dispersion direction.

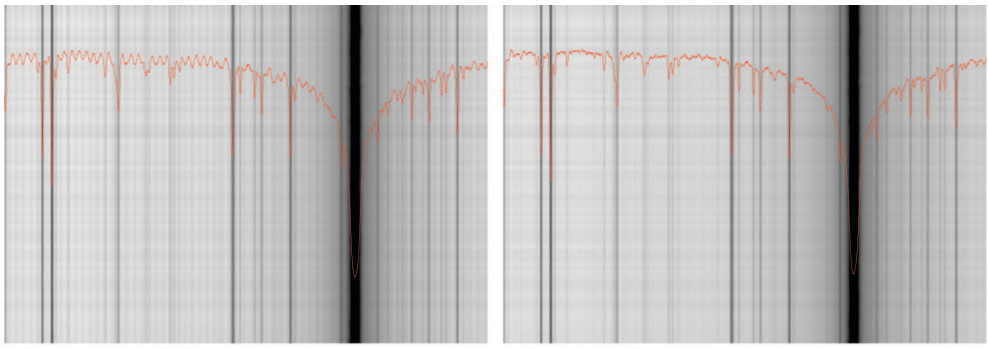

Fig. 14 *Left*: A flat-fielded Hα 2D spectral image and the spectral profile superposed on it. *Right*: The de-fringed result of the spectrum on the left by subtracting the reconstructed fringe pattern from the flat-fielded spectrum. The spectral profile is also over plotted on it.

subtracted from the flat-fielded object data to eliminate the residual fringe. The final 1D spectrum superposed on the 2D result is exhibited in the right panel of Figure 14.

Here we need to point out that in spite of the efficient performance of the above two methods, these approaches, from the point view of "software," may result in some artificial features. For example, in Figure 12, an arrow indicates the disappearance of one weak absorption line due to de-fringing. In the NVST, we are also making efforts to eliminate the problem of fringing from the camera itself. We will not discuss that work here since it is beyond the scope of this paper.

4 CONCLUSIONS

The present work is dedicated to building standard data reduction routines for the high-dispersion spectral data taken with NVST's Multi-wavelength Spectrometer. We summarize all the steps in a flow chart shown in Figure 15. Based on the primary data reduction, we draw the following conclusions about the main properties of the spectral observation using the Multi-wavelength Spectrometer, providing a reference for future observations.

(1) Background frames can be conveniently and safely acquired by covering the entrance slit at the end of the daily observation. 20 frames with an exposure of 20 ms are sufficient to construct the dark field.
(2) Flat-field source frames and object data should be taken at close intervals, particularly considering the time evolution of the fringe.

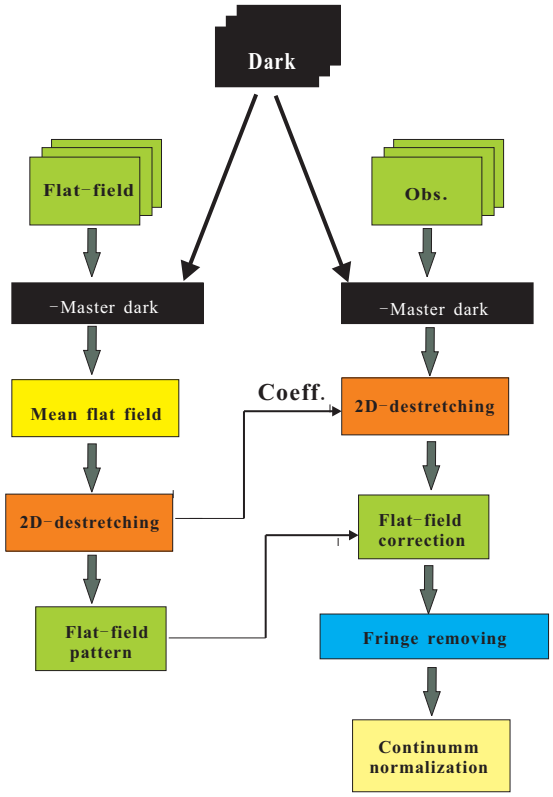

Fig. 15 The flow chart of the whole data reduction process.

(3) The most important step is to rectify the spectral image in two dimensions. Moreover, both the *mean flat-field source frame* and object data have to be de-stretched in exactly the same way. Our experiments and trials demonstrate that it is essential to have a sufficient number of source frames to extract a flat field with sufficient quality. Using the Multi-wavelength Spectrometer, about 200 frames are acceptable for both the Hα and Ca II 8542 Å lines.
(4) After dark field subtraction and flat-field reduction, sometimes an extra treatment is needed to eliminate the residual fringe in the reduced data. Two methods are applied and compared. One is to use the standard solar spectral atlas as a reference. The other is based on the wavelet analysis of the *mean profile*. However, both of them may introduce artificial features to some weak absorption lines.
(5) Wavelength calibration of the reduced data based on the FTS atlas reveals that the spectral sample of this spectrometer is about 0.011 Å pixel^{-1}, close to the expectation considering the optical design. Given the assumption that the instrument profile caused by aberrations in the optical system follow a Gaussian profile, we computationally infer that the upper limit of the FWHM for the instrumental profile is about 0.065 Å. It can be ignored if the Hα or Ca II 8542 Å lines are used to extract the physical parameters (e.g., the temperature and electron density).

Acknowledgements The authors wish to thank Tai Guo, Shan-Jie Huang and Lei Yang for their kind assistance with the operation of the NVST. Many thanks to Fang-Yu Xu for his fruitful discussion. NSO/Kitt Peak FTS data used in this paper were produced by NSF/NOAO. This work is partially supported by the National Natural Science Foundation of China (Grant No. 11103075) and the West Light Foundation of Chinese Academy of Sciences.

References

Allende Prieto, C., Asplund, M., & Fabiani Bendicho, P. 2004, A&A, 423, 1109
Bommier, V., & Molodij, G. 2002, A&A, 381, 241
Bommier, V., & Rayrole, J. 2002, A&A, 381, 227
Fu, Y., Chen, X.-M., Yuan, S., & Xu, Z. 2012, CJL, 39, SII, *http://www.opticsjournal.net/Abstract.htm?aid=OJ121231000189pWsYv2*
Hall, J. C., Fulton, E. E., Huenemoerder, D. P., Welty, A. D., & Neff, J. E. 1994, PASP, 106, 315
Howell, S. B. 2006, Handbook of CCD Astronomy (2nd ed.; New York: Cambridge Univ. Press)
Johanneson, A., Bida, T., Lites, B., & Scharmer, G. B. 1992, A&A, 258, 572
Kiselman, D. 1994, A&AS, 104, 23
Liu, Z., & Xu, J. 2011, 1-meter Near-infrared Solar Telescope, in Astronomical Society of India Conference Series, 2, eds. A. R. Choudhuri, & D. Banerjee, 9
Malumuth, E. M., Hill, R. S., Gull, T., et al. 2002, Removing Fringes from STIS Slitless Spectra and WFC3 CCD Images, 2002 (HST Calibration Workshop)
Pereira, T. M. D., Kiselman, D., & Asplund, M. 2009, A&A, 507, 417
Rojo, P. M., & Harrington, J. 2006, ApJ, 649, 553
Scodeggio, M., Franzetti, P., Garilli,B., et al. 2005, PASP, 117, 837
Wöhl, H., Kučera, A., Rybák, J., & Hanslmeier, A. 2002, A&A, 394, 1077